Report

Cell Reports

Essential Structural and Functional Roles of the Cmr4 Subunit in RNA Cleavage by the Cmr CRISPR-Cas Complex

Graphical Abstract

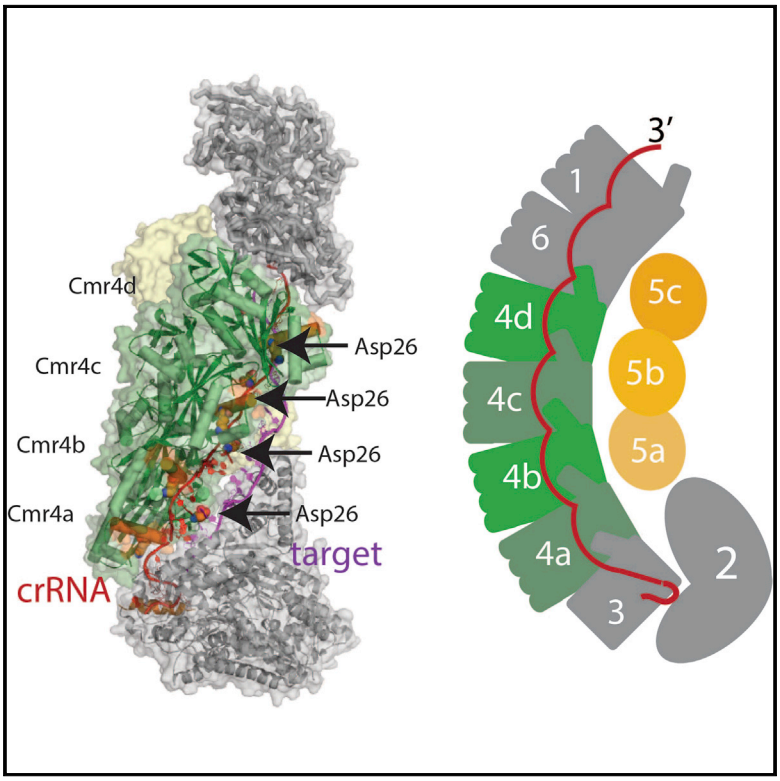

Authors

Nancy F. Ramia, Michael Spilman, ..., Hong Li, Scott M. Stagg

Correspondence

mterns@bmb.uga.edu (M.P.T.),
hong.li@fsu.edu (H.L.),
sstagg@fsu.edu (S.M.S.)

In Brief

Ramia et al. show that the helical core of the type III-B Cmr CRISPR-Cas effector complex, made up of multiple Cmr4 subunits, forms the platform for a corresponding number of cleavages of the target RNA. Comparison with the type I-E Cascade structure reveals strikingly similar mechanisms of crRNA and target binding.

Highlights

Cmr4 subunits form the backbone of the Cmr CRISPR-Cas complex

Mutations in Cmr4 abolish target RNA cleavage

Hook structures in the four Cmr4 subunits form four potential cleavage sites

Cmr crRNA and target-binding mechanism resemble the Cascade complex

Accession Numbers

EMD-6165
EMD-6166
EMD-6167
4RDP

Ramia et al., 2014, Cell Reports 9, 1610–1617
December 11, 2014 ©2014 The Authors
http://dx.doi.org/10.1016/j.celrep.2014.11.007

CrossMark

CellPress

OPEN ACCESS
CellPress

Cell Reports
Report

Essential Structural and Functional Roles of the Cmr4 Subunit in RNA Cleavage by the Cmr CRISPR-Cas Complex

Nancy F. Ramia,[1] Michael Spilman,[1] Li Tang,[1] Yaming Shao,[1] Joshua Elmore,[3] Caryn Hale,[3] Alexis Cocozaki,[1] Nilakshee Bhattacharya,[1] Rebecca M. Terns,[3] Michael P. Terns,[3,*] Hong Li,[1,2,*] and Scott M. Stagg[1,2,*]
[1]Institute of Molecular Biophysics, Florida State University, Tallahassee, FL 32306, USA
[2]Department of Chemistry and Biochemistry, Florida State University, Tallahassee, FL 32306, USA
[3]Departments of Biochemistry and Molecular Biology, Genetics, and Microbiology, University of Georgia, Athens, GA 30602, USA
*Correspondence: mterns@bmb.uga.edu (M.P.T.), hong.li@fsu.edu (H.L.), sstagg@fsu.edu (S.M.S.)
http://dx.doi.org/10.1016/j.celrep.2014.11.007
This is an open access article under the CC BY-NC-ND license (http://creativecommons.org/licenses/by-nc-nd/3.0/).

SUMMARY

The Cmr complex is the multisubunit effector complex of the type III-B clustered regularly interspaced short palindromic repeats (CRISPR)-Cas immune system. The Cmr complex recognizes a target RNA through base pairing with the integral CRISPR RNA (crRNA) and cleaves the target at multiple regularly spaced locations within the complementary region. To understand the molecular basis of the function of this complex, we have assembled information from electron microscopic and X-ray crystallographic structural studies and mutagenesis of a complete *Pyrococcus furiosus* Cmr complex. Our findings reveal that four helically packed Cmr4 subunits, which make up the backbone of the Cmr complex, act as a platform to support crRNA binding and target RNA cleavage. Interestingly, we found a hook-like structural feature associated with Cmr4 that is likely the site of target RNA binding and cleavage. Our results also elucidate analogies in the mechanisms of crRNA and target molecule binding by the distinct Cmr type III-A and Cascade type I-E complexes.

INTRODUCTION

The clustered regularly interspaced short palindromic repeats (CRISPR)-CRISPR-associated proteins (Cas) system is a recently described adaptive immune system in prokaryotes that targets invading phages and plasmids using short RNA as guides (Barrangou and Marraffini, 2014; Terns and Terns, 2011; van der Oost et al., 2014). Three types of CRISPR-Cas systems carry out the target interference process (Makarova et al., 2011a), in which a transcribed and fully processed CRISPR RNA (crRNA) is assembled with a surveillance/effector protein or protein complex (CRISPR ribonucleoproteins [crRNPs]). Nucleic acid targets are captured by the crRNA through base pairing and cleaved via the effector protein(s) or factors associated with the surveillance complex. The target interference complexes of types I, II, and III differ in their RNA and protein composition (Makarova et al., 2011a). Whereas type II complexes are comprised of a single effector protein (Gasiunas et al., 2012; Jinek et al., 2012), those of types I and III contain multiple protein subunits (Brouns et al., 2008; Hale et al., 2009; Hatoum-Aslan et al., 2014; Sinkunas et al., 2013; Wiedenheft et al., 2011a).

The multicomponent type I and III crRNPs contain members of the large subunit (Cas8 for type I and Cas10 for type III), the small subunit, Cas5, and Cas7 superfamilies of proteins (Hale et al., 2009; Hatoum-Aslan et al., 2014; Rouillon et al., 2013; Spilman et al., 2013; Staals et al., 2013). Cas10 proteins contain an adenylyl-cyclase-like domain that is often fused with an amino terminal histidine-aspartate (HD) domain related to those found in DNA-cleaving enzymes (Makarova et al., 2013). Cas8 and Cas10 proteins are large in size but do not share sequence homology. Cas5 and Cas7 are both repeat-associated mysterious proteins (RAMPs) characterized by the presence of the ferredoxin-like fold (Makarova et al., 2011b). Recently, important structural insights were gained from 3D electron microscopy (3DEM) (Rouillon et al., 2013; Spilman et al., 2013; Staals et al., 2013; Wiedenheft et al., 2011a), X-ray crystallographic (Jackson et al., 2014; Mulepati et al., 2014; Zhao et al., 2014), and modeling (Benda et al., 2014) studies of type I-E (Cascade) and type III-A (Csm) and III-B (Cmr) crRNPs. Despite their distant phylogeny, the type I and III crRNPs share a similar helical architecture and structural homology in individual subunits, particularly Cas5 and Cas7. High-resolution structures of the type I-E Cascade show that both Cas5 and Cas7 form a set of regularly spaced clamps that secure the bound cRNA (Jackson et al., 2014; Mulepati et al., 2014; Zhao et al., 2014). The guide:target heteroduplex stabilized in this manner deviates drastically from the standard forms and is unwound every sixth base pair, which is believed to facilitate segmented target binding (Mulepati et al., 2014). In contrast to the detailed mechanism of the type I crRNPs, the mechanism of nucleic acid binding for the type III crRNPs remains unknown.

The type III-B Cmr complex targets RNA for destruction (Benda et al., 2014; Hale et al., 2009, 2012; Staals et al., 2013; Zhang et al., 2012) and generally contains six Cmr proteins, Cmr1–Cmr6. Cmr1, Cmr4, and Cmr6 belong to the Cas7

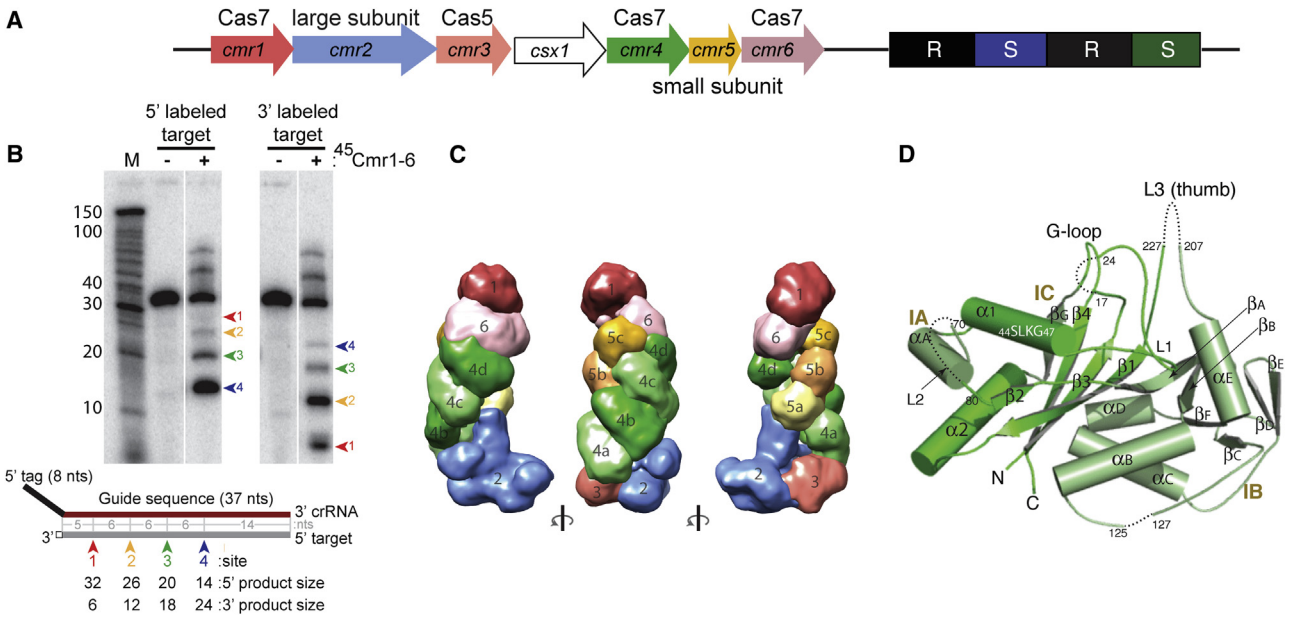

Figure 1. Overview of *Pyrococcus furiosus cmr* Gene Arrangement, Activity of the Cmr Complex EM Specimens, EM Structure of the Cmr Complex, and Crystal Structure of the Cmr4 Subunit

(A) The arrangement of *cmr* genes in relationship to CRISPR repeats (R) and spacers (S).

(B) Target RNA cleavage activity of the full-length Cmr complex used for EM studies. Diagrammed is the crRNA with 8 nt 5′ tag (black) and 37 nt guide (orange) duplexed with the 37 nt complementary target RNA (gray) with additional 3′-labeled nucleotide indicated (white square). The cleavage sites observed and corresponding products of cleavage of 5′- and 3′-radiolabeled target RNAs are indicated with colored and numbered arrows.

(C) EM structures of the holo Cmr complex with 45 nt crRNA and 37 nt target RNA. Colors represent density segmentations of the Cmr1–Cmr6 complex highlighting individual subunits. Three different views are shown, and densities for each of the subunits are resolved and are labeled.

(D) Crystal structure of Cmr4. Secondary structural elements are labeled numerically for the core ferredoxin-like fold and alphabetically for insertion elements. Insertion segments are named IA, IB, and IC and their locations indicated by dashed boxes in the topology diagram (Figure S2). Disordered regions are indicated by dashed curves.

superfamily, Cmr3 belongs to the Cas5 superfamily, and Cmr2 and Cmr5 are the large (Cas10) and small subunit, respectively (Makarova et al., 2011a; Figure 1A). Studies with *Pyrococcus furiosus* (Pf) and *Thermus thermophilus* (Tt) Cmr complexes showed that the Cmr complex is associated with predominantly two forms of the crRNA that differ by six nucleotides in length (Hale et al., 2009; Staals et al., 2013) and, interestingly, cleaves the target RNA at multiple sites (without a requirement for an exogenous nuclease), also with a six-nucleotide spacing (Hale et al., 2014; Staals et al., 2013; Figure 1B). The *Sulfolobus solfataricus* Cmr complex contains an additional Cmr7 protein and has significantly different RNA cleavage properties than the Pf and Tt Cmr complexes (Zhang et al., 2012).

Previously determined 3DEM structures of an in vivo isolated *Tt* Cmr complex and of a reconstituted *Pf* Cmr complex lacking the HD domain at the amino terminus of its Cmr2 subunit found that Cmr4 comprises the central backbone of the Cmr complex but has different stoichiometries in the two Cmr complexes (Spilman et al., 2013; Staals et al., 2013). On the other hand, a recent modeling study of the *Pf* Cmr complex, in which crystal structures of the six subunits were docked to the 3DEM density of the *Pf* Cmr complex lacking the HD domain, suggested that the *Pf* and the *Tt* Cmr complexes have the same Cmr4 stoichiometry (Benda et al., 2014). Cmr4 is known to be present along the length of the guide region of the crRNA, where target interaction and cleavage occurs (Spilman et al., 2013); however, the molecular basis of Cmr4 interaction with the crRNA or the target RNA remains unknown.

In this work, we have purified and reconstituted the *Pf* Cmr complex using the full-length Cmr2 (full-length Cmr complex herein) and obtained an electron microscopy (EM) structure using single-particle reconstruction. Furthermore, we obtained a crystal structure of *Pf* Cmr4 at 2.8 Å resolution that recapitulates the arrangement and interactions of the central backbone of the full-length complex. The combined EM and X-ray crystallographic studies resulted in a consistent model of the *Pf* Cmr complex at an atomic resolution and revealed Cmr4-associated features suggestive of RNA cleavage centers. Mutagenesis studies identified structural elements of Cmr4 essential for crRNA binding as well as target RNA cleavage. Comparison of the Cmr complex structure to the crystal structure of the Cascade complex showed an analogous mechanism of crRNA and target RNA binding between the two different types of crRNPs.

RESULTS

Overview of the Full-Length Cmr Complex Structure

Reconstituted and functional full-length Cmr complexes (Figures S1A and 1B) were subjected to 3DEM analysis. To ensure

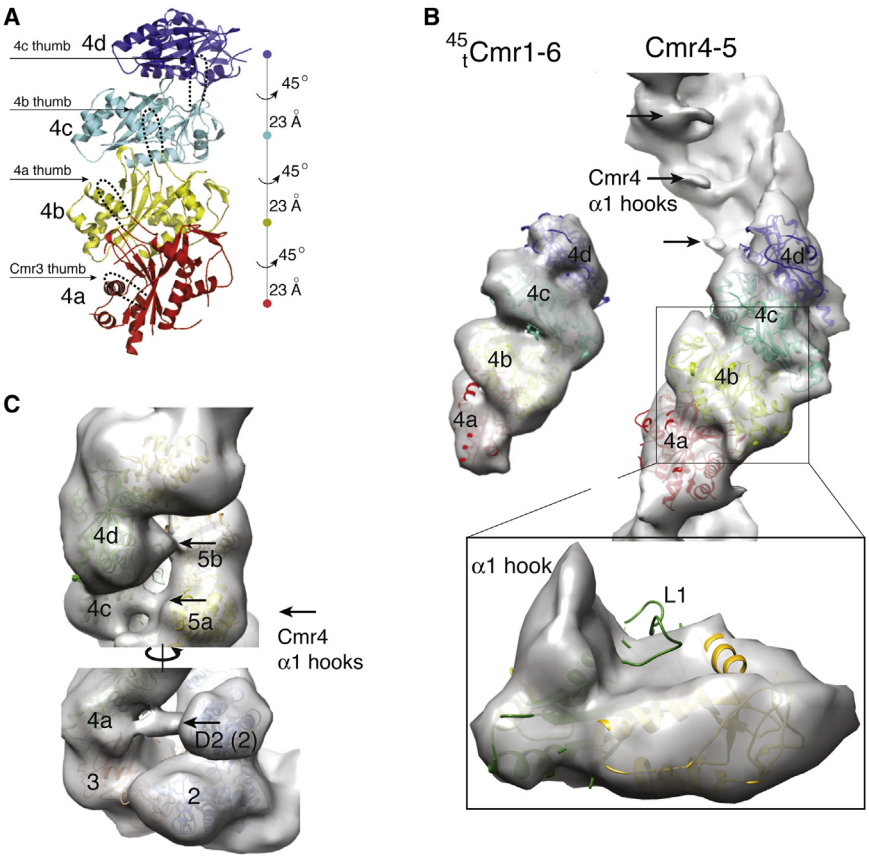

Figure 2. Fitting of Cmr4 Crystal Structure to EM Densities and Detailed View of α1 Hooks

(A) The Cmr4 filament generated by crystallographic and noncrystallographic symmetries. Cmr4 monomers (red, yellow, cyan, and blue) are related by an 8-fold rotation and a 23 Å translation. The disordered β-hairpin (whose equivalent in Cascade is termed thumb) is indicated by dashed lines. The dashed lines also indicate that the thumb of the preceding Cmr4 likely interacts with the α1 helix of the following Cmr4.

(B) Rigid-body fit of four packed Cmr4 molecules to the density of the central body of the 3DEM structure of the full-length Cmr complex ($^{45}_{t}$Cmr1–Cmr6) and that of the high-resolution structure of the Cmr4–Cmr5 filament (Cmr4–Cmr5), where the density belonging to Cmr5 was removed for clarity. Inset shows a close up of Cmr4 crystal structure fitting to the density of the Cmr4–Cmr5 filament. The protruding EM density near α1 (α1 hook) is unaccounted for by the crystal structure but may accommodate the loop L1, which correspondingly is found in a position in the crystal structure lacking EM density.

(C) Two different views of the full-length Cmr complex density reveal the arrangement of the α1 hooks. Note that the α1 hook of Cmr4a connects to the D2 domain of Cmr2 whereas those of Cmr4b, Cmr4c, and Cmr4d connect to Cmr5 subunits.

accurate subunit assignment and detect conformational changes, negative stain EM data sets were collected for each of the three Cmr complex samples: Cmr1–Cmr6 with 45 nucleotide crRNA and target RNA ($^{45}_{t}$Cmr1–Cmr6), Cmr1–Cmr6 with 45 nucleotide crRNA alone (^{45}Cmr1–Cmr6), and Cmr2–Cmr6 with 45 nucleotide crRNA (^{45}Cmr2–Cmr6; Figure S1C). In addition, a cryoEM data set was collected for isolated Cmr4–Cmr5 protein filament (Figure S1C). The three data sets of full Cmr complexes were reconstructed in three dimensions using single-particle refinement to better than 15 Å resolution, and that of the Cmr4–Cmr5 filament was refined to better than 12 Å by helical reconstruction (Figure S1C; Table S1; Supplemental Experimental Procedures).

The full-length Cmr complex bound with the 45 nt crRNA and the target RNA resulted in clear density features for segmentation (Figure 1C). Subunits could be unambiguously assigned to segments by a combination of difference map and crystal-structure-fitting methods (Figures S1C and S3; Supplemental Experimental Procedures). In addition, the helically reconstructed Cmr4–Cmr5 filament clearly matches the central repeats of the intact complex (Figure 2). The final stoichiometry of the full-length Cmr complex assembled with 45 nt crRNA and a complementary target is $Cmr1_1$:$Cmr2_1$:$Cmr3_1$:$Cmr4_4$:$Cmr5_3$:$Cmr6_1$:$crRNA_1$ (Figure 1C). The new density unobserved in the truncated Cmr2 crystal structure was assigned to the HD domain of Cmr2 (Figure S1C).

An Atomic Resolution View of the Central Body

The central backbone structure of the Cmr complex was further analyzed by a 2.8 Å crystal structure of the Cmr4 subunit (Table S2). Remarkably, both crystallographic and noncrystallographic packing of Cmr4 generates an infinite filament with a nearly perfect 8-fold screw symmetry (45° rotation with a 23 Å translational interval along the helical axis) that recapitulates the structure of the central backbone of the Cmr complex (Figures 2A and 2B). Four head-to-tail-packed Cmr4 molecules could be readily fit into the density belonging to the central backbone of the Cmr complex or the Cmr4–Cmr5 filament with minor adjustments (Figure 2B). The structural model of the Cmr complex was completed by placing structures of three helically assembled Cmr5 subunits (Park et al., 2013), the Cmr2–Cmr3 heterocomplex, and the homologs of Cmr6 (Cmr4) and Cmr1 (afCmr1) into the EM density of the fully assembled Cmr complex (Figure 2B). Docking the crystal structures of these Cmr subunits to the previous EM density map lacking the Cmr2 HD domain led to a similar model (Benda et al., 2014).

Comparison of the Cmr4 crystal structure with its corresponding EM density in the higher resolution cryoEM structure of isolated Cmr4–Cmr5 filament revealed a protruding density (α1 hook) that emerges from α1 of each Cmr4 and extends across the major helical groove to Cmr5 (or Cmr2 for Cmr4a; Figure 2C). The Cmr4-associated α1 hook serves as the front gate of the

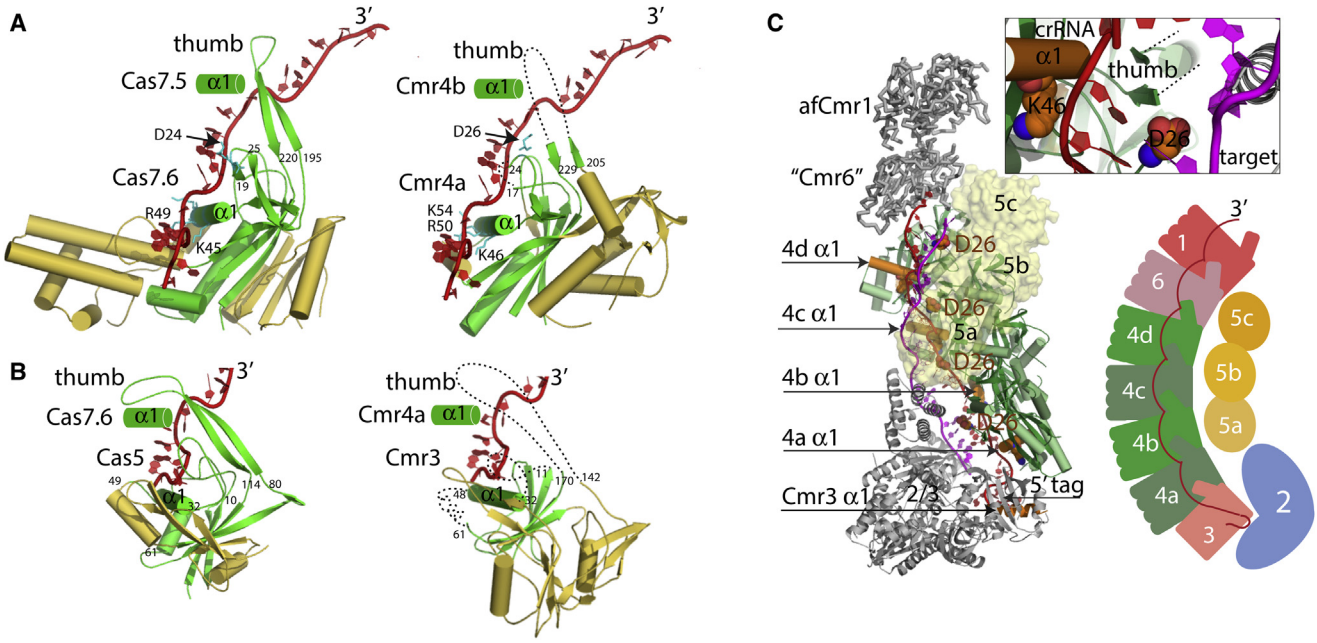

Figure 3. Structural Similarity between Subunits of the Cmr and the Cascade Complexes Suggests an RNA-Binding Model

(A) Superimposed Cmr4 and Cas7 (Cas7.6) structures displayed side by side. The crRNA bound to Cas7.6 is shown in red and also modeled with Cmr4. The core ferredoxin-like fold of each protein is colored in green, and the rest is colored in yellow orange. Numbers indicate residue numbers, and dashed lines mark disordered regions. The α1 helix from the upper adjoining Cas7 subunit in assembled Cascade or Cmr is schematically shown as a green cylinder. Conserved residues on loop L1 and α1 helix that play roles in anchoring the crRNA in Cas7 are shown in stick models for both Cas7 and Cmr4.

(B) Superimposed Cmr3 and Cas5 structures displayed side by side. The crRNA bound to Cas7 is modeled with both Cas5 and Cmr3 (shown in red). The core ferredoxin-like fold of each protein is colored in green, and the rest is colored in yellow orange. Numbers indicate residue numbers, and dashed lines mark disordered regions.

(C) 3DEM density-fitted atomic structure of the Cmr complex. Crystal structures of Pf Cmr2–Cmr3 (PDB ID: 4H4K), Cmr5 (PDB ID: 4GKF), Cmr4 (PDB ID: 4RDP), and *Archaeoglobus fulgidus* Cmr1 (afCmr1) (PDB ID: 4L6U) were fitted into the EM density of the full-length Cmr complex. Cmr6 is approximated using the structure of Cmr4 ("Cmr6"). Cmr2 and Cmr3 are shown in gray ribbons, Cmr5 subunits are displayed as surface models, Cmr1 and Cmr6 as simple ribbon models, and Cmr4 subunits are displayed as cartoons. The α1 helix of each Cmr4 and that of Cmr3 are colored in orange. Lys46 and Asp26 are shown in orange spheres. The partial crRNA-target model associated with Cmr5 and Cmr4 (red and magenta) was generated from that bound to the homologous Cas7 in Cascade using the symmetry relating Cmr4 subunits. Inset illustrates structural features around the α1 hook density. A cartoon model representing the organization and crRNA binding of the Cmr complex is displayed using the same coloring scheme as in Figure 1.

Cmr complex and may control access of crRNA and/or target RNA to the interior of the central helical body.

Homologous Structural Elements Suggest Similar crRNA and Target-Binding Models for Cmr and Cascade Complexes

Superimposition of Pf Cmr4 and Pf Cmr5 with the analogous *E. coli* type I-E Cascade complex subunits, Cas7 and Cas5, respectively (Jackson et al., 2014; Mulepati et al., 2014; Zhao et al., 2014), revealed striking structural homology that suggests a similar RNA-binding mechanism (Figures 3A and 3B). In Cascade, Cas7 uses a characteristic β-hairpin (thumb) to form a clamp with the α1 helix (palm) of its neighboring Cas7 subunit to secure the crRNA in a sequence-independent manner (Figure 3A). The Cas5 and the Cas7.6 subunit (closest to Cas5) form the first composite site (Figure 3B). The analogous elements of Pf Cmr4 would be in place to form the same thumb-palm clamps provided its β-hairpin thumb is ordered upon assembly (Figures 2A and 3A). Similarly, Pf Cmr3 and Cmr4a would form the first thumb-palm clamp (Figures 2A and 3B).

Guided by the predicted RNA-binding elements of Cmr4, we built a Cmr4-bound nucleic acid model from the guide:target heteroduplex bound to Cascade (Mulepati et al., 2014). We assumed that the heteroduplex segment (five base pairs plus two unpaired bases) associated with Cas7.6 of Cascade binds similarly to Cmr4a, which allowed us to generate three additional heteroduplex segments bound to Cmr4b, Cmr4c, and Cmr4d by applying the same symmetry relating the four Cmr4 proteins to the heteroduplex segments (Figure 3C). With minor adjustments, the four heteroduplex segments can be connected into intact strands that represent a model of crRNA:single-stranded DNA bound with the Cmr complex (Figure 3C). The junction of two heteroduplex segments coincides with the observed α1 hook and the projected path of the β-hairpin thumb of Cmr4 (Figure 3C, inset). At the analogous locations in Cascade, an Asp-Arg/Lys-Trp triad is observed that bridges two consecutive Cas7 subunits and the small subunit (or Cas8; Zhao et al., 2014). Equivalent residues that are capable of participating in a triad bridge are also found at this location in Cmr4 (Asp26 and Trp226), although Trp226 is disordered and the accurate orientation of Cmr5 could

not be determined. When the Cmr4-nucleic acid model is fit into the EM map for the full-length Cmr complex bound with the 45 nt crRNA and target RNA, the crRNA model is partially contained within the density, whereas the target RNA model is largely outside the density (Figure S3). Our Cmr complex preparations clearly show the presence of the RNAs (Figures S1A and S1B), suggesting the possibility that the path of the Cmr crRNA deviates from that bound to Cascade, the crRNA dissociates during EM preparation, or the crRNA is only weakly bound to the complex. The striking homology between the central backbone of the Cmr complex and that of Cascade strongly argues that the nucleic acid duplex bound to the Cmr complex also likely remains flat and stretched (Mulepati et al., 2014). Furthermore, the Cmr guide:target duplex is likely also unwound at six base pair intervals in accord with the analogous β-hairpin thumbs near the α1 hooks of the Cmr4 subunits (Figure 3C, inset).

Mutations in Cmr4 Abolish Target RNA Cleavage

Previous structural and crosslinking data point to Cmr4 as the most likely catalytic subunit of the Cmr complex. Our model (Figure 3C), based on the structural analogy with Cascade and biochemical evidence including protein-crRNA UV-crosslinking data (Spilman et al., 2013), indicates that the four self-oligomerized Cmr4 subunits of the helical backbone of the intact Cmr complex can make direct contact with portions of the crRNA guide element, which base pairs with regions of the target RNA where four cleavages occur at regular 6 nt intervals. We assayed the effects of several mutations of Cmr4 on both target RNA cleavage activity (Figures 4A, 4C, and 4D) and crRNA-binding/Cmr complex formation (Figures 4B and 4E). The conserved Cmr4 residues targeted for alanine substitution mutagenesis included a histidine residue (H15) that was earlier predicted to be a key active site residue (Makarova et al., 2011b) as well as several other conserved residues (R31, D26, E32, T35, K46, R50, D86A, R112, R209, E227/E228, and K276) with potential to perform acid/base catalysis typical for facilitating cleavage of phosphodiester bonds (see Cmr4 sequence alignment; Figure S4). Most of the tested Cmr4 mutants did not result in any discernible effects on target RNA cleavage or crRNA binding (Figures 4A and 4B). (However, note a weak but consistent effect on both of these activities for double mutation Cmr4 E227A, E228A of the β-hairpin thumb). In contrast, cleavage was abolished by mutation of both K46A of the α1 helix (Figure 4A) and D26A (or D26N) of the potential triad bridge region of Cmr4 (Figures 4C and 4D).

The effect of the Cmr4 K46A mutation on target RNA cleavage was accompanied by a loss of crRNA association/Cmr complex formation, indicating that K46 plays a critical role in crRNA interaction (Figure 4B). In contrast, the Cmr4 D26A (and D26N) mutation resulted in a specific loss of all four target RNA cleavages (Figures 4C and 4D) without any detectable loss of crRNA association/Cmr complex assembly (Figure 4E) or target RNA association (Figure 4F). (Note that a low level of spurious cleavage near target RNA site 2 was reproducibly observed [Figures 4C and 4D; data not shown].) Our findings indicate that Cmr4 D26 is directly important for target RNA cleavage, consistent with a similar finding by Benda et al. (2014). The close proximity of D26 to the α1 hook and its potential relationship with the Cascade Asp-Arg/Lys-Trp triad suggest that this region is the center of target RNA cleavage.

DISCUSSION

Combined EM, crystallographic, and mutagenesis analysis produced a detailed model for assembly and function of the Cmr complex. Furthermore, comparison of the structures of analogous subunits in the type I-E Cascade complex revealed analogous nucleic-acid-binding methods. The structure of the crRNA-target RNA duplex bound to the Cmr complex likely deviates from the standard A form and contains regularly disrupted base pairs. The discontinuous crRNA-target RNA-binding model with 6 bp segments may underlie the multiple cleavages catalyzed by the Cmr complex at 6 nt intervals (Hale et al., 2014; Staals et al., 2013; Figure 1B).

The potential coincidence of Cmr4-associated α1 hooks with junctions of the guide:target model and the predicted Asp(26)-Arg/Lys-Trp triad suggests their involvement in RNA binding and possibly in catalysis. Our mutagenesis data support this hypothesis and indicate that Cmr4 (a Cas7 superfamily member) is the primary source of the nuclease activity of the Cmr complex. It remains to be determined, though, why alteration of the D26 residue of Cmr4 subunit leads to loss of target RNA cleavages. The D26 residue may function as part of a specific set of Cmr4 active site residues yet to be defined that facilitates target RNA cleavage through general acid-base chemistry or via coordination with a catalytic divalent metal ion. Alternatively, target RNA cleavage may occur by an autocatalytic mechanism (Ferré-D'Amaré and Scott, 2010; Lilley, 2011), facilitated by a specific target RNA interaction involving Cmr4 D26. The active site residues may distort target nucleotides, which favors in-line attack by a nucleophilic 2′-OH. A lack of crRNA-target RNA pairing in the vicinity of the predicted target RNA cleavage site, as is observed in type I-E effector complexes (Mulepati et al., 2014; Wiedenheft et al., 2011b) may precede or accompany the postulated Cmr4-target base interaction.

The crystal structure of Cmr4 expands the repertoire of structures of Cas7 proteins (this study and Benda et al. 2014). Unlike the related Cas6 family of RAMP proteins, all Cas7 structures reveal a single ferredoxin-like fold interrupted by large insertions or extensions (Figure S5). Cmr4 represents the first type III-B Cas7 structure (Cmr1 is more similar to Cas6 family proteins), and its structure reveals several differences from type III-A (Csm3 and Csa2) and type I-E (Cas7/Cse4/CasC) Cas7 proteins, primarily in the location and structures of the insertion elements. The two conserved regions among Cas7 proteins, the α1 helix and the β-hairpin thumb, cofunction in crRNA binding and target positioning. Our finding that a Cmr4 K46A mutation within the conserved $_{44}$SLKG$_{47}$ motif of the Cas7 superfamily of proteins (see Figure S4) abolished crRNA interaction is consistent with the close association of α1 with the crRNA and the reported importance in crRNA binding in other type I and III crRNPs (Hrle et al., 2013; Lintner et al., 2011; Figure 3).

EXPERIMENTAL PROCEDURES

Protein Purification and Cmr Complex Reconstitution

The Cmr proteins other than Cmr2 were purified as previously described (Spilman et al., 2013). The full-length Cmr2 was purified using a similar

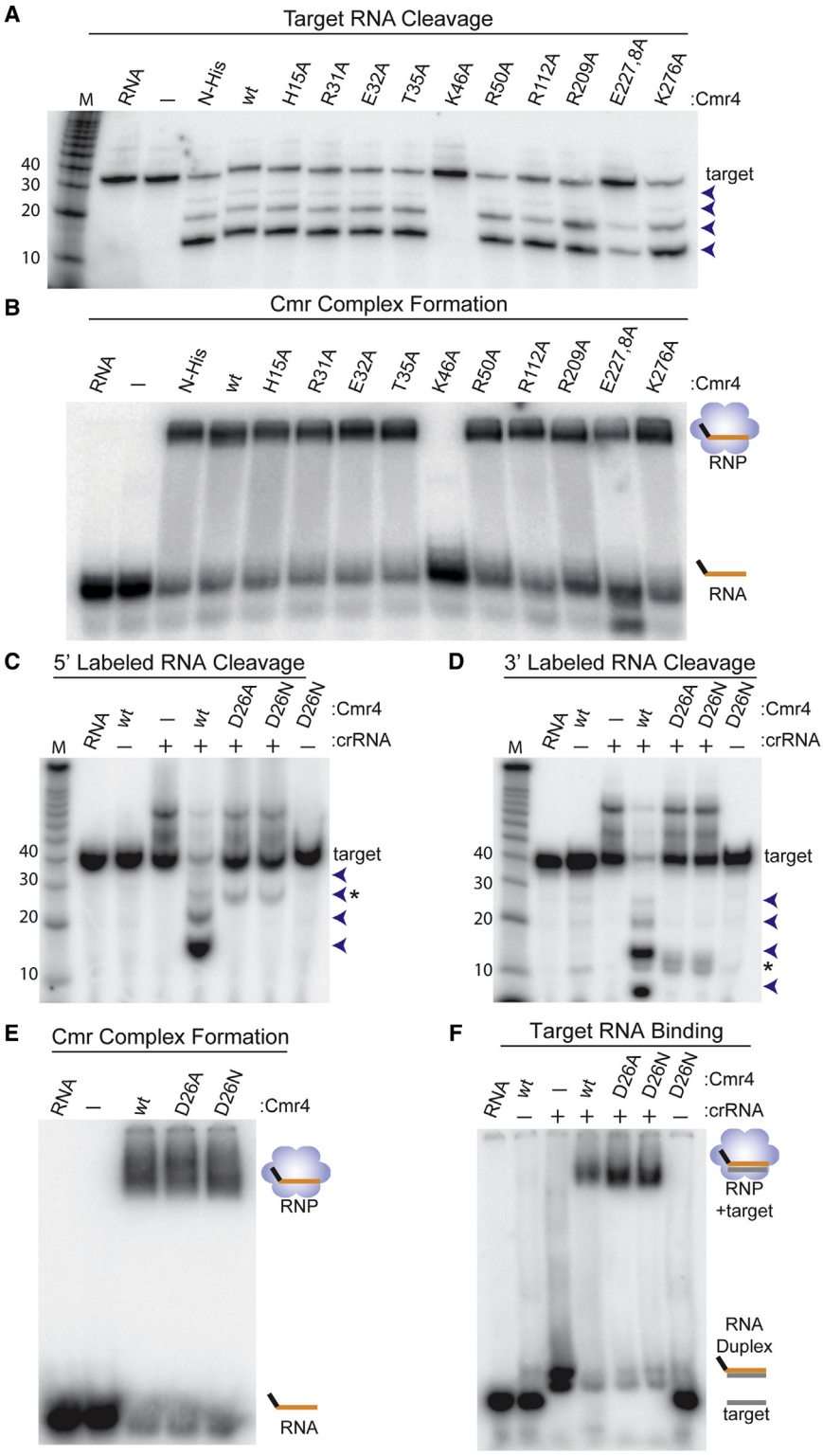

Figure 4. Effects of Cmr4 Mutations on Cleavage Activity and Complex Formation

(A) Target RNA cleavage by Cmr complexes with mutant Cmr4 subunits. Cmr complexes with indicated mutants, wild-type, or without Cmr4 (–) were incubated with radiolabeled target RNA, and products were analyzed by denaturing gel electrophoresis. Target RNA alone (RNA) is also shown. Radiolabeled Decade marker RNAs were used for size determination (M). Positions of the four 5′-labeled target RNA cleavage products are indicated (arrowheads). wt, wild-type.

(B and E) crRNP formation by Cmr complexes with mutant Cmr4 subunits. 3′ end-labeled 45 nt crRNA binding by Cmr complexes with indicated mutant Cmr4 subunits was analyzed by native gel electrophoresis. The positions of the crRNA (RNA) and crRNA-Cmr protein complex (RNP) are indicated.

(C and D) Target RNA cleavage by Cmr complexes with D26 mutant Cmr4 subunits. Complexes containing the indicated Cmr4, formed with (+) or without (–) 45 nt crRNA, were incubated with 5′ end-labeled (C) or 3′ end-labeled (D) target RNA. Positions of the four 5′- and 3′-labeled target RNA wild-type Cmr cleavage products are indicated (arrowheads). A spurious cleavage product observed with the mutants is also indicated (asterisk).

(F) Target RNA binding by Cmr complexes with D26 mutant Cmr4 subunits. Complexes containing the indicated Cmr4, formed with (+) or without (–) 45 nt crRNA, were incubated with 5′ end-labeled target RNA and analyzed by native gel electrophoresis. The positions of the target RNA (target), duplexed target RNA-crRNA (RNA duplex), and Cmr RNP + target (RNP + target) are indicated.

procedure with slight modifications. Detailed methods can be found in the Supplemental Experimental Procedures. Briefly, Cmr4, Cmr5, and Cmr6 were purified as a ternary subcomplex and Cmr1 or Cmr3 were purified independently using a Ni-nitrilotriacetic acid column followed by a size-exclusion column. The full complex was assembled by incubation with a crRNA and isolated by a size-exclusion method.

Electron Microscopy Reconstruction of the Cmr Complexes

Purified Cmr complexes were studied by negative stain. Detailed methods of sample preparation and data collection and analysis are included in the Supplemental Experimental Procedures. Briefly, the negative stained samples were prepared using 2% (w/v) uranyl formate and data collected with an FEI Titan Krios using the automatic data acquisition software Leginon (Suloway et al., 2005). Particles were picked by an automated difference-of-Gaussians picker using an iterative method and were reconstructed using a combination of projection matching (Ludtke et al., 1999) and multivariate data analysis (Frank et al., 1996). Resolutions for all reconstructions were determined by Fourier shell correlation and cross-validated by both independent refinement of half sets (Scheres, 2012) and Fourier neighbor correlation as implemented in the program RMEASURE (Sousa and Grigorieff, 2007; Supplemental Experimental Procedures). Long filaments of the Cmr4–Cmr5 complex were prepared for cryoEM by heating a

sample of Cmr4–Cmr5 to 70°C for 15 min and cooling to room temperature over 10 min. The helical reconstruction of Cmr4–Cmr5 was accomplished using the iterative helical reconstruction method (Egelman, 2010) combined with EMAN and in-house software. The initial model for refinement was a filled featureless cylinder with the same diameter as the filaments and the 24.7 Å rise and 48.2° twist of the filament were from the previous Cmr4–Cmr5 structure in negative stain (Spilman et al., 2013).

Crystal Structure Determination of Cmr4

PfCmr4 was purified as described above and crystallized using a hanging drop vapor diffusion method. Selenomethionine-substituted sample was used to obtain single-wavelength diffraction data, which led to structure determination and refinement at 2.8 Å. Diffraction data and refinement statistics are included in Table S2.

Cmr4 Mutant Analysis: crRNA Binding, Target RNA Binding, and Cleavage Assays

Cmr4 mutants were generated by site-directed mutagenesis, and the proteins were purified as described above. To assemble Cmr4 mutant-containing Cmr complexes, individually purified Cmr proteins lacking Cmr4 were incubated with each Cmr4 mutant protein. For crRNA-binding assays, the Cmr protein mixtures were incubated with γ^{32}P-ATP 5′ end-labeled crRNA and then resolved on a native gel. For target cleavage, the same complexes were first assembled with a nonlabeled crRNA and subsequently with either the 5′ (γ^{32}P-ATP) or 3′ (^{32}PCp) end-labeled target RNA. Cleavage products were visualized on a denaturing gel. Detailed methods are included in the Supplemental Experimental Procedures.

ACCESSION NUMBERS

The negative-stained Cmr complex EM map was deposited in the EM databank under the accession numbers EMD-6165 and EMD-6166 (sharpened). The cryoEM structure of the Cmr4-5 filament was deposited under the accession number EMD-6167. The crystal structure of Cmr4 was deposited in the Protein Data Bank (PDB) database under the accession number 4RDP.

SUPPLEMENTAL INFORMATION

Supplemental Information includes Supplemental Experimental Procedures, five figures, and two tables and can be found with this article online at http://dx.doi.org/10.1016/j.celrep.2014.11.007.

AUTHOR CONTRIBUTIONS

N.F.R. purified and reconstituted the complexes for EM studies. M.S., N.B., and S.M.S. collected and processed EM data, Y.S. and L.T. determined crystal structures; J.E., C.H., A.C., R.M.T., and M.P.T. conceived and carried out mutagenesis and functional analysis; and R.M.T., M.P.T., S.M.S., and H.L. wrote the manuscript.

ACKNOWLEDGMENTS

This work was supported by NIH grant R01 GM99604 to H.L., American Heart Association predoctoral fellowship 11PRE7090000 to A.C., and NIH grant R01 GM54682 to M.P.T. and R.M.T.

Received: September 8, 2014
Revised: October 14, 2014
Accepted: November 5, 2014
Published: December 4, 2014

REFERENCES

Barrangou, R., and Marraffini, L.A. (2014). CRISPR-Cas systems: Prokaryotes upgrade to adaptive immunity. Mol. Cell *54*, 234–244.

Benda, C., Ebert, J., Scheltema, R.A., Schiller, H.B., Baumgärtner, M., Bonneau, F., Mann, M., and Conti, E. (2014). Structural Model of a CRISPR RNA-Silencing Complex Reveals the RNA-Target Cleavage Activity in Cmr4. Mol. Cell *56*, 43–54.

Brouns, S.J., Jore, M.M., Lundgren, M., Westra, E.R., Slijkhuis, R.J., Snijders, A.P., Dickman, M.J., Makarova, K.S., Koonin, E.V., and van der Oost, J. (2008). Small CRISPR RNAs guide antiviral defense in prokaryotes. Science *321*, 960–964.

Egelman, E.H. (2010). Reconstruction of helical filaments and tubes. Methods Enzymol. *482*, 167–183.

Ferré-D'Amaré, A.R., and Scott, W.G. (2010). Small self-cleaving ribozymes. Cold Spring Harb. Perspect. Biol. *2*, a003574.

Frank, J., Radermacher, M., Penczek, P., Zhu, J., Li, Y., Ladjadj, M., and Leith, A. (1996). SPIDER and WEB: processing and visualization of images in 3D electron microscopy and related fields. J. Struct. Biol. *116*, 190–199.

Gasiunas, G., Barrangou, R., Horvath, P., and Siksnys, V. (2012). Cas9-crRNA ribonucleoprotein complex mediates specific DNA cleavage for adaptive immunity in bacteria. Proc. Natl. Acad. Sci. USA *109*, E2579–E2586.

Hale, C.R., Zhao, P., Olson, S., Duff, M.O., Graveley, B.R., Wells, L., Terns, R.M., and Terns, M.P. (2009). RNA-guided RNA cleavage by a CRISPR RNA-Cas protein complex. Cell *139*, 945–956.

Hale, C.R., Majumdar, S., Elmore, J., Pfister, N., Compton, M., Olson, S., Resch, A.M., Glover, C.V., 3rd, Graveley, B.R., Terns, R.M., and Terns, M.P. (2012). Essential features and rational design of CRISPR RNAs that function with the Cas RAMP module complex to cleave RNAs. Mol. Cell *45*, 292–302.

Hale, C.R., Cocozaki, A., Li, H., Terns, R.M., and Terns, M.P. (2014). Target RNA capture and cleavage by the Cmr type III-B CRISPR-Cas effector complex. Genes Dev. *28*, 2432–2443.

Hatoum-Aslan, A., Maniv, I., Samai, P., and Marraffini, L.A. (2014). Genetic characterization of antiplasmid immunity through a type III-A CRISPR-Cas system. J. Bacteriol. *196*, 310–317.

Hrle, A., Su, A.A., Ebert, J., Benda, C., Randau, L., and Conti, E. (2013). Structure and RNA-binding properties of the type III-A CRISPR-associated protein Csm3. RNA Biol. *10*, 1670–1678.

Jackson, R.N., Golden, S.M., van Erp, P.B., Carter, J., Westra, E.R., Brouns, S.J., van der Oost, J., Terwilliger, T.C., Read, R.J., and Wiedenheft, B. (2014). Structural biology. Crystal structure of the CRISPR RNA-guided surveillance complex from Escherichia coli. Science *345*, 1473–1479.

Jinek, M., Chylinski, K., Fonfara, I., Hauer, M., Doudna, J.A., and Charpentier, E. (2012). A programmable dual-RNA-guided DNA endonuclease in adaptive bacterial immunity. Science *337*, 816–821.

Lilley, D.M. (2011). Catalysis by the nucleolytic ribozymes. Biochem. Soc. Trans. *39*, 641–646.

Lintner, N.G., Kerou, M., Brumfield, S.K., Graham, S., Liu, H., Naismith, J.H., Sdano, M., Peng, N., She, Q., Copié, V., et al. (2011). Structural and functional characterization of an archaeal clustered regularly interspaced short palindromic repeat (CRISPR)-associated complex for antiviral defense (CASCADE). J. Biol. Chem. *286*, 21643–21656.

Ludtke, S.J., Baldwin, P.R., and Chiu, W. (1999). EMAN: semiautomated software for high-resolution single-particle reconstructions. J. Struct. Biol. *128*, 82–97.

Makarova, K.S., Haft, D.H., Barrangou, R., Brouns, S.J., Charpentier, E., Horvath, P., Moineau, S., Mojica, F.J., Wolf, Y.I., Yakunin, A.F., et al. (2011a). Evolution and classification of the CRISPR-Cas systems. Nat. Rev. Microbiol. *9*, 467–477.

Makarova, K.S., Aravind, L., Wolf, Y.I., and Koonin, E.V. (2011b). Unification of Cas protein families and a simple scenario for the origin and evolution of CRISPR-Cas systems. Biol. Direct *6*, 38.

Makarova, K.S., Wolf, Y.I., and Koonin, E.V. (2013). The basic building blocks and evolution of CRISPR-CAS systems. Biochem. Soc. Trans. *41*, 1392–1400.

Mulepati, S., Héroux, A., and Bailey, S. (2014). Structural biology. Crystal structure of a CRISPR RNA-guided surveillance complex bound to a ssDNA target. Science *345*, 1479–1484.

Park, J.H., Sun, J., Park, S.Y., Hwang, H.J., Park, M.Y., Shin, M., and Kim, J.S. (2013). Crystal structure of Cmr5 from Pyrococcus furiosus and its functional implications. FEBS Lett. *587*, 562–568.

Rouillon, C., Zhou, M., Zhang, J., Politis, A., Beilsten-Edmands, V., Cannone, G., Graham, S., Robinson, C.V., Spagnolo, L., and White, M.F. (2013). Structure of the CRISPR interference complex CSM reveals key similarities with cascade. Mol. Cell *52*, 124–134.

Scheres, S.H. (2012). RELION: implementation of a Bayesian approach to cryo-EM structure determination. J. Struct. Biol. *180*, 519–530.

Sinkunas, T., Gasiunas, G., Waghmare, S.P., Dickman, M.J., Barrangou, R., Horvath, P., and Siksnys, V. (2013). In vitro reconstitution of Cascade-mediated CRISPR immunity in Streptococcus thermophilus. EMBO J. *32*, 385–394.

Sousa, D., and Grigorieff, N. (2007). Ab initio resolution measurement for single particle structures. J. Struct. Biol. *157*, 201–210.

Spilman, M., Cocozaki, A., Hale, C., Shao, Y., Ramia, N., Terns, R., Terns, M., Li, H., and Stagg, S. (2013). Structure of an RNA silencing complex of the CRISPR-Cas immune system. Mol. Cell *52*, 146–152.

Staals, R.H., Agari, Y., Maki-Yonekura, S., Zhu, Y., Taylor, D.W., van Duijn, E., Barendregt, A., Vlot, M., Koehorst, J.J., Sakamoto, K., et al. (2013). Structure and activity of the RNA-targeting Type III-B CRISPR-Cas complex of Thermus thermophilus. Mol. Cell *52*, 135–145.

Suloway, C., Pulokas, J., Fellmann, D., Cheng, A., Guerra, F., Quispe, J., Stagg, S., Potter, C.S., and Carragher, B. (2005). Automated molecular microscopy: the new Leginon system. J. Struct. Biol. *151*, 41–60.

Terns, M.P., and Terns, R.M. (2011). CRISPR-based adaptive immune systems. Curr. Opin. Microbiol. *14*, 321–327.

van der Oost, J., Westra, E.R., Jackson, R.N., and Wiedenheft, B. (2014). Unravelling the structural and mechanistic basis of CRISPR-Cas systems. Nat. Rev. Microbiol. *12*, 479–492.

Wiedenheft, B., Lander, G.C., Zhou, K., Jore, M.M., Brouns, S.J., van der Oost, J., Doudna, J.A., and Nogales, E. (2011a). Structures of the RNA-guided surveillance complex from a bacterial immune system. Nature *477*, 486–489.

Wiedenheft, B., van Duijn, E., Bultema, J.B., Waghmare, S.P., Zhou, K., Barendregt, A., Westphal, W., Heck, A.J.R., Boekema, E.J., Dickman, M.J., and Doudna, J.A. (2011b). RNA-guided complex from a bacterial immune system enhances target recognition through seed sequence interactions. Proc. Natl. Acad. Sci. USA *108*, 10092–10097.

Zhang, J., Rouillon, C., Kerou, M., Reeks, J., Brugger, K., Graham, S., Reimann, J., Cannone, G., Liu, H., Albers, S.V., et al. (2012). Structure and mechanism of the CMR complex for CRISPR-mediated antiviral immunity. Mol. Cell *45*, 303–313.

Zhao, H., Sheng, G., Wang, J., Wang, M., Bunkoczi, G., Gong, W., Wei, Z., and Wang, Y. (2014). Crystal structure of the RNA-guided immune surveillance Cascade complex in Escherichia coli. Nature *515*, 147–150.